

VOLUME OPTIMAL CYCLE: TIGHTEST REPRESENTATIVE CYCLE OF A GENERATOR ON PERSISTENT HOMOLOGY

IPPEI OBAYASHI

ABSTRACT. This paper shows a mathematical formalization, algorithms and computation software of volume optimal cycles, which are useful to understand geometric features shown in a persistence diagram. Volume optimal cycles give us concrete and optimal homologous structures, such as rings or cavities, on a given data. The key idea is the optimality on $(q + 1)$ -chain complex for a q th homology generator. This optimality formalization is suitable for persistent homology. We can solve the optimization problem using linear programming. For an alpha filtration on \mathbb{R}^n , volume optimal cycles on an $(n - 1)$ -th persistence diagram is more efficiently computable using merge-tree algorithm. The merge-tree algorithm also gives us a tree structure on the diagram and the structure has richer information. The key mathematical idea is Alexander duality.

1. INTRODUCTION

Topological Data Analysis (TDA) [1, 2], which clarifies the geometric features of data from the viewpoint of topology, is developed rapidly in this century both in theory and application. In TDA, persistent homology and its persistence diagram (PD) [3, 4] are important tool for TDA. Persistent homology enables us to capture multiscale topological features effectively and quantitatively. Fast computation softwares for persistent homology are developed [5, 6] and many applications are achieved such as materials science [7, 8, 9], sensor networks [10], evolutions of virus [11], and so on. From the viewpoint of data analysis, a PD has some significant properties: translation and rotation invariance, multiscalability and robustness to noise. PDs are considered to be compact descriptors for complicated geometric data.

q th homology H_q encodes q dimensional geometric structures of data such as connected components ($q = 0$), rings ($q = 1$), cavities ($q = 2$), etc. q th persistent homology encodes the information about q dimensional geometric structures with their scale. A PD, a multiset¹ in $\mathbb{R} \times (\mathbb{R} \cup \{\infty\})$, is used to summarize the information. Each point in a PD is called a birth-death pair, which represents a homologous structure in the data, and the scale is encoded on x-axis and y-axis.

Typical workflow of the data analysis with persistent homology is as follows:

- (1) Construct a filtration from data
 - Typical input data is a point cloud, a finite set of points in \mathbb{R}^n and a typical filtration is an alpha filtration
- (2) Compute the PD from the filtration
- (3) Analyze the PD to investigate the geometric features of the data

In the last part of the above workflow, we often want to inversely reconstruct a geometric structure corresponding each birth-death pair on the PD, such as a ring or a cavity, into the original input data. Such inverse analysis is practically important for the use of PDs. For example, we consider the 1st PD shown in Fig. 1 from the atomic configuration of amorphous silica computed by molecular dynamical

¹A multiset is a set with multiplicity on each point.

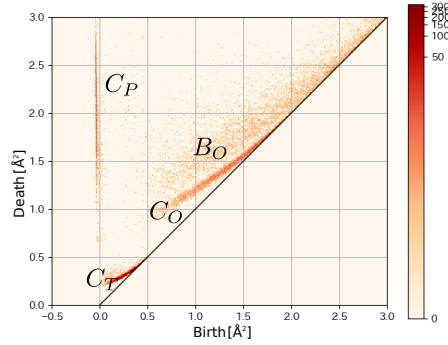


FIGURE 1. The 1st PD for the atomic configuration of amorphous silica in [7], reproduced from the simulation data. The data is provided by Dr. Nakamura.

simulation [7]. In this PD, there are some characteristic bands C_P, C_T, C_O, B_O , and these bands correspond to typical geometric structures in amorphous silica. To analyze the PD more deeply, we want to reconstruct rings corresponding such birth-death pairs in the original data. In the paper, optimal cycles, one of such inverse analysis methods, are effectively used to clarify such typical structures.

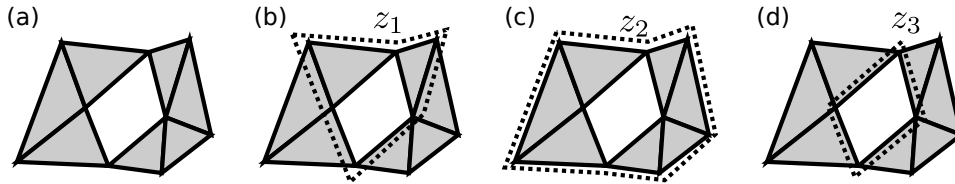


FIGURE 2. A simplicial complex with one hole.

A representative cycle of a generator of the homology vector space has such information, but it is not unique and we want to find a better cycle to understand the homology generator for the analysis of a PD. For example, Fig. 2(a) has one homology generator on H_1 , and cycles z_1, z_2 , and z_3 shown in Fig. 2 (b), (c), and (d) are the same homologous information. However, we consider that z_3 is best to understand the homology. Optimization problems on homology are used to find such a representative cycle. We can find the “tightest” representative cycle under a certain formalization. Such optimization problems have been widely studied under various settings[12, 13, 14], and two concepts, optimal cycles[15] and volume optimal cycles[16], have been successfully applied to persistent homology. The optimal cycle minimizes the size of the cycle, while the volume optimal cycle minimizes the internal volume of the cycle. Both of these two methods give a tightest cycle in different senses. The volume optimal cycles for persistent homology have been proposed in [16] under the restriction of dimension. We can use them only for $(n - 1)$ -th persistent homology embedded in \mathbb{R}^n , but under the restriction, there is an efficient computation algorithm using Alexander duality.

In this paper, we generalize the concept of volume optimal cycles on any persistent homology and show the computation algorithm. The idea in [16] is not applied to find a volume optimal ring (a volume optimal cycle for $q = 1$) in a point cloud in \mathbb{R}^3 but our method is applicable to such a case. In that case, optimal cycles are

also applicable, but our new algorithm is simpler, faster for large data, and gives us better information.

The contributions of this paper are as follows:

- The concept of volume optimal cycles is proposed to identify good representatives of generators in persistent homology. This is useful to understand a persistence diagram.
 - The concept has been already proposed in [16] in a strongly limited sense about dimension and this paper generalize it.
 - Optimal cycles are also usable for the same purpose, but the algorithm in this paper is easier to implement, faster, and gives better information.
 - * Especially, children birth-death pairs shown in Section 6 are available only with volume optimal cycles.
- Mathematical properties of volume optimal cycles are clarified.
- Effective computation algorithms for volume optimal cycles are proposed.
- The algorithm is implemented and some examples are computed by the program to show the usefulness of volume optimal cycles.

The rest of this paper is organized as follows. The fundamental ideas such as persistent homology and simplicial complexes are introduced in Section 2. In Section 3 the idea of optimal cycles is reviewed. Section 4 is the main part of the paper. The idea of volume optimal cycles and the computation algorithm in a general setting are presented in Section 4. Some mathematical properties of volume optimal cycles are also shown in this section. In Section 5 we show some special properties of $(n - 1)$ -th persistent homology in \mathbb{R}^n and the faster algorithm. We also explain tree structures in $(n - 1)$ -th persistent homology. In Section 6, we compare volume optimal cycles and optimal cycles. In Section 7 we show some computational examples by the proposed algorithms. In Section 8, we conclude the paper.

2. PERSISTENT HOMOLOGY

In this section, we explain some preliminaries about persistent homology and geometric models. Persistent homology is available on various general settings, but we mainly focus on the persistent homology on a filtration of simplicial complexes, especially an alpha filtration given by a point cloud.

2.1. Persistent homology. Let $\mathbb{X} = \{X_t \mid t \in T\}$ be a *filtration* of topological spaces where T is a subset of \mathbb{Z} or \mathbb{R} . That is, $X_t \subset X_{t'}$ holds for every $t \leq t'$. Then we define q th homology vector spaces $\{H_q(X_t)\}_{t \in T}$ whose coefficient is a field \mathbb{k} and homology maps $\varphi_s^t : H_q(X_s) \rightarrow H_q(X_t)$ for all $s \leq t$ induced by inclusion maps $X_s \hookrightarrow X_t$. The family $H_q(\mathbb{X}) = (\{H_q(X_t)\}_t, \{\varphi_s^t\}_{s \leq t})$ is called the q th *persistent homology*. The theory of persistent homology enables us to analyze the structure of this family.

Under some assumptions, $H_q(\mathbb{X})$ is uniquely decomposed as follows [3, 4]:

$$H_q(\mathbb{X}) = \bigoplus_{i=1}^p I(b_i, d_i),$$

where $b_i \in T, d_i \in T \cup \{\infty\}$ with $b_i < d_i$. Here, $I(b, d) = (U_t, f_s^t)$ consists of a family of vector spaces and linear maps:

$$U_t = \begin{cases} \mathbb{k}, & \text{if } b \leq t < d, \\ 0, & \text{otherwise,} \end{cases}$$

$$f_s^t : U_s \rightarrow U_t$$

$$f_s^t = \begin{cases} \text{id}_{\mathbb{k}}, & \text{if } b \leq s \leq t < d, \\ 0, & \text{otherwise.} \end{cases}$$

This means that for each $I(b_i, d_i)$ there is a q dimensional hole in \mathbb{X} and it appears at $t = b_i$, persists up to $t < d_i$ and disappears at $t = d_i$. In the case of $d_i = \infty$, the q dimensional hole never disappears on \mathbb{X} . b_i is called a *birth time*, d_i is called a *death time*, and the pair (b_i, d_i) is called a *birth-death pair*. When \mathbb{X} is a filtration of finite simplicial/cell/cubical complexes on T with $\#T < \infty$ (we call \mathbb{X} a *finite filtration* under the condition), such a unique decomposition exists.

When we have the unique decomposition, the q th *persistence diagram* of \mathbb{X} , $D_q(\mathbb{X})$, is defined by a multiset

$$D_q(\mathbb{X}) = \{(b_i, d_i) \mid i = 1, \dots, p\},$$

and the 2D scatter plot or the 2D histogram of $D_q(\mathbb{X})$ is often used to visualize the diagram.

We investigate the detailed algebraic structure of persistent homology for the preparation. For simplicity, we assume the following condition on \mathbb{X} .

Condition 1. Let $X = \{\sigma_1, \dots, \sigma_K\}$ be a finite simplicial complex. For any $1 \leq k \leq K$, $X_k = \{\sigma_1, \dots, \sigma_k\}$ is a subcomplex of X .

Under the condition,

$$(1) \quad \mathbb{X} : \emptyset = X_0 \subset X_1 \subset \dots \subset X_K = X,$$

is a filtration of complexes. For a general finite filtration, we can construct a filtration satisfying Condition 1 by ordering all simplices properly. Let $\partial_q : C_q(X) \rightarrow C_{q-1}(X)$ be the boundary operator on $C_q(X)$ and $\partial_q^{(k)} : C_q(X_k) \rightarrow C_{q-1}(X_k)$ be a boundary operator of $C_q(X_k)$. Cycles $Z_q(X_k)$ and boundaries $B_q(X_k)$ are defined by the kernel of $\partial_q^{(k)}$ and the image of $\partial_{q+1}^{(k)}$, and q th homology vector spaces are defined by $H_q(X_k) = Z_q(X_k)/B_q(X_k)$. Condition 1 says that if σ_k is a q -simplex,

$$(2) \quad \begin{aligned} C_q(X_k) &= C_q(X_{k-1}) \oplus \langle \sigma_k \rangle, \\ C_{q'}(X_k) &= C_{q'}(X_{k-1}), \text{ for } q' \neq q, \end{aligned}$$

holds. From the decomposition theorem and (2), for each birth-death pair (b_i, d_i) , we can find $z_i \in C_q(X)$ such that

$$(3) \quad z_i \notin Z_q(X_{b_i-1}),$$

$$(4) \quad z_i \in Z_q(X_{b_i}) = Z_q(X_{b_i-1}) \oplus \langle \sigma_{b_i} \rangle,$$

$$(5) \quad z_i \notin B_q(X_k) \text{ for } k < d_i,$$

$$(6) \quad z_i \in B_q(X_{d_i}) = B_q(X_{d_i-1}) \oplus \langle \partial \sigma_{d_i} \rangle,$$

$$(7) \quad \{[z_i]_k \mid b_i \leq k < d_i\} \text{ is a basis of } H_q(X_k),$$

where $[z]_k = [z]_{B_q(X_k)} \in H_q(X_k)$. (6) holds only if $d_i \neq \infty$. This $[z_i]_k$ is a homology generator that persists from $k = b_i$ to $k = d_i - 1$. $\{z_i\}_{i=1}^p$ is called the *persistence cycles* for $D_p(\mathbb{X}) = \{(b_i, d_i)\}_{i=1}^p$. An algorithm of computing a PD actually finds persistence cycles from a given filtration. The persistence cycle of (b_i, d_i) is not unique, therefore we want to find a ‘‘good’’ persistence cycle to find out the geometric structure corresponding to each birth-death pair. That is the purpose

of the volume optimal cycle, which is the main topic of this paper. We remark that the condition (7) can be easily proved from (3-6) and the decomposition theorem, and hence we only need to show (3-6) to prove that given $\{z_i\}_{i=1}^P$ are persistence cycles.

2.2. Alpha filtration. One of the most used filtrations for data analysis using persistent homology is an alpha filtration [2, 17]. An alpha filtration is defined from a point cloud, a set of finite points $P = \{x_i \in \mathbb{R}^n\}$. The alpha filtration is defined as a filtration of alpha complexes and they are defined by a Voronoi diagram and a Delaunay triangulation.

The *Voronoi diagram* for a point cloud P , which is a decomposition of \mathbb{R}^n into *Voronoi cells* $\{V(x_i) \mid x_i \in P\}$, is defined by

$$V(x_i) = \{x \in \mathbb{R}^n \mid \|x - x_i\|_2 \leq \|x - x_j\|_2 \text{ for any } j \neq i\}.$$

The *Delaunay triangulation* of P , $\text{Del}(P)$, which is a simplicial complex whose vertices are points in P , is defined by

$$\text{Del}(P) = \{[x_{i_1} \cdots x_{i_q}] \mid V(x_{i_1}) \cap \cdots \cap V(x_{i_q}) \neq \emptyset\},$$

where $[x_{i_0} \cdots x_{i_q}]$ is the q -simplex whose vertices are $x_{i_0}, \dots, x_{i_q} \in P$. Under the assumption of general position in the sense of [17], the Delaunay triangulation is a simplicial decomposition of the convex hull of P and it has good geometric properties. The *alpha complex* $\text{Alp}(P, r)$ with radius parameter $r \geq 0$, which is a subcomplex of $\text{Del}(P)$, is defined as follows:

$$\text{Alp}(P, r) = \{[x_{i_0} \cdots x_{i_q}] \in \text{Del}(P) \mid B_r(x_{i_0}) \cap \cdots \cap B_r(x_{i_q}) \neq \emptyset\},$$

where $B_r(x)$ is the closed ball whose center is x and whose radius is r . A significant property of the alpha complex is the following homotopy equivalence to the r -ball model.

$$\bigcup_{x_i \in P} B_r(x_i) \simeq |\text{Alp}(P, r)|,$$

where $|\text{Alp}(P, r)|$ is the geometric realization of $\text{Alp}(P, r)$. The *alpha filtration* for P is defined by $\{\text{Alp}(P, r)\}_{r \geq 0}$. Figure 3 illustrates an example of a filtration by r -ball model and the corresponding alpha filtration. The 1st PD of this filtration is $\{(r_2, r_5), (r_3, r_4)\}$. Since there are $r_1 < \cdots < r_K$ such that $\text{Alp}(P, s) = \text{Alp}(P, t)$ for any $r_i \leq s < t < r_{i+1}$, we can treat the alpha filtration as a finite filtration $\text{Alp}(P, r_1) \subset \cdots \subset \text{Alp}(P, r_K)$.

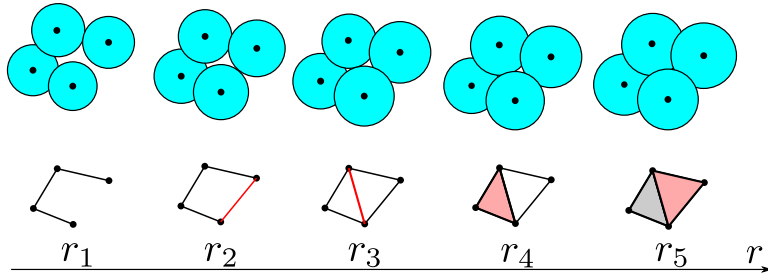


FIGURE 3. An r -ball model and the corresponding alpha filtration. Each red simplex in this figure appears at the radius parameter r_i .

We mention an weighted alpha complex and its filtration [18]. An alpha complex is topologically equivalent to the union of r -balls, while an weighted alpha complex is topologically equivalent to the union of $\sqrt{r^2 + \alpha_i}$ -balls, where α_i depends on each point. The weighted alpha filtration is useful to study the geometric structure of

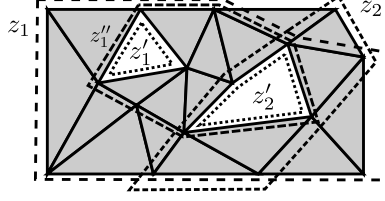


FIGURE 4. A simplicial complex with two holes.

a point cloud whose points have their own radii. For example, for the analysis of atomic configuration, the square of ionic radii or Van der Waals radii are used as α_i .

3. OPTIMAL CYCLE

First, we discuss an optimal cycle on normal homology whose coefficient is $\mathbb{k} = \mathbb{Z}_2$. Figure 2(a) shows a simplicial complex whose 1st homology vector space H_1 is isomorphic to \mathbb{Z}_2 . In Fig. 2(b), (c), and (d), z_1 , z_2 , and z_3 have same information about H_1 . That is, $H_1 = \langle [z_1] \rangle = \langle [z_2] \rangle = \langle [z_3] \rangle$. However, we intuitively consider that z_3 is the best to represent the hole in Fig. 2 since z_3 is the shortest loop in these loops. Since the size of a loop $z = \sum_{\sigma: 1\text{-simplex}} \alpha_\sigma \sigma \in Z_1(X)$ is equal to

$$\#\{\sigma : 1\text{-simplex} \mid \alpha_\sigma \neq 0\},$$

and this is ℓ^0 “norm”²³, we write it $\|z\|_0$. Here, z_3 is the solution of the following problem:

$$\text{minimize } \|z\|_0, \text{ subject to } z \sim z_1.$$

The minimizing z is called the *optimal cycle* for z_1 . From the definition of homology, we can rewrite the problem as follows:

$$(8) \quad \begin{aligned} &\text{minimize } \|z\|_0, \text{ subject to:} \\ &z = z_1 + \partial w, \\ &w \in C_2(X). \end{aligned}$$

Now we complete the formalization of the optimal cycle on a simplicial complex with one hole.

How about the case if a complex has two or more holes? We consider the example in Fig. 4. From z_1 and z_2 , we try to find z_1' and z_2' using a similar formalization. If we apply the optimization (8) to each z_1 and z_2 , z_1' and z_2' are found. How can we find z_1' from z_1 and z_2 ? The problem is a hole represented by z_2' , therefore we “fill” that hole and solve the minimization problem. Mathematically, filling a hole corresponds to considering $Z_1(X)/(B_1(X) \oplus \langle z_2' \rangle)$ instead of $Z_1(X)/B_1(X)$ and the following optimization problem gives us the required loop z_1' .

$$\begin{aligned} &\text{minimize } \|z\|_0, \text{ subject to:} \\ &z = z_1 + \partial w + kz_2', \\ &w \in C_2(X), \\ &k \in \mathbb{Z}_2. \end{aligned}$$

² For a finite dimensional \mathbb{R} - or \mathbb{C} - vector space whose basis is $\{g_i\}_i$, the ℓ^0 norm $\|\cdot\|_0$ is defined by $\|\sum_i \alpha_i g_i\|_0 = \#\{i \mid \alpha_i \neq 0\}$. Mathematically this is not a norm since it is not homogeneous, but in information science and statistics, it is called ℓ^0 norm.

³ On a \mathbb{Z}_2 -vector space, any norm is not defined mathematically, but it is natural that we call this ℓ^0 norm.

When you have a complex that has many holes, you can apply the idea repeatedly to find all optimal cycles. The idea of optimal cycles obviously applied q th homology for any q .

3.1. How to compute an optimal cycle. Finding a basis of a homology vector space is not a difficult problem for a computer. We prepare a matrix representation of the boundary operator and apply matrix reduction algorithm. Please read [19] for the detailed algorithm. Therefore the problem is how to solve the above minimizing problem.

In general, solving a optimization problem on a \mathbb{Z}_2 linear space is a difficult problem. The problem is a kind of combinatorial optimization problems. They are well studied but it is well known that such a problem is sometimes hard to solve on a computer.

One approach is using linear programming, used in [20]. Since optimization problem on \mathbb{Z}_2 is hard, we use \mathbb{R} as a coefficient. For \mathbb{R} coefficient, ℓ^0 norm also means the size of loop and ℓ^0 optimization is natural for our purpose. However, ℓ^0 optimization is also a difficult problem. Therefore we replace ℓ^0 norm to ℓ^1 norm. It is well known in the fields of sparse sensing and machine learning that ℓ^1 optimization gives a good approximation of ℓ^0 optimization. That is, we solve the following optimization problem instead of (8).

$$(9) \quad \begin{aligned} &\text{minimize } \|z\|_1, \text{ subject to:} \\ &z = z_1 + \partial w, \\ &w \in C_2(X; \mathbb{R}). \end{aligned}$$

This is called a linear programming and we can solve the problem very efficiently by good solvers such as cplex⁴ and Clp⁵.

Another approach is using integer programming, used in [12, 15]. ℓ^1 norm optimization gives a good approximation, but maybe the solution is not exact. However, if all coefficients are restricted into 0 or ± 1 in the optimization problem (9), the ℓ^0 norm and ℓ^1 norm is identical, and it gives a better solution. This restriction on the coefficients has another advantage that we can understand the optimal solution in more intuitive way. Such an optimization problem is called integer programming. Integer programming is much slower than linear programming, but some good solvers such as cplex and Clp are available for integer programming.

3.2. Optimal cycle for a filtration. Now, we explain optimal cycles on a filtration to analyze persistent homology shown in [15]. We start from the example Fig. 5.

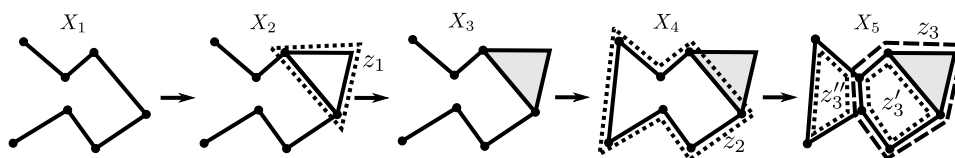


FIGURE 5. A filtration example for optimal cycles.

In the filtration, a hole $[z_1]$ appears at X_2 and disappear at X_3 , another hole $[z_2]$ appears at X_4 and $[z_3]$ appears at X_5 . The 1st PD of the filtration is $\{(2, 3), (4, \infty), (5, \infty)\}$.

⁴<https://www-01.ibm.com/software/commerce/optimization/cplex-optimizer/>

⁵<https://projects.coin-or.org/Clp>

The persistence cycles z_1, z_2, z_3 , are computable by the algorithm of persistent homology and we want to find z'_3 or z''_3 to analyze the hole corresponding to the birth-death pair $(5, \infty)$. The hole $[z_1]$ has been already dead at X_5 and $[z_2]$ remains alive at X_5 , so we can find z'_3 or z''_3 to solve the following optimization problem:

$$\begin{aligned} & \text{minimize } \|z\|_0 \text{ subject to:} \\ & z = z_3 + \partial w + kz_2, \\ & w \in C_1(X_5), \\ & k \in \mathbb{k}. \end{aligned}$$

In this case, z''_3 is chosen because $\|z'_3\|_0 > \|z''_3\|_0$. By generalizing the idea, we show Algorithm 1 to find optimal cycles for a filtration \mathbb{X} ⁶. Of course, to solve the optimization problem in Algorithm 1, we can use the computation techniques shown in Section 3.1.

Algorithm 1 Computation of optimal cycles on a filtration

Compute $D_q(\mathbb{X})$ and persistence cycles z_1, \dots, z_n
 Choose $(b_i, d_i) \in D_q(\mathbb{X})$ by a user
 Solve the following optimization problem

$$\begin{aligned} & \text{minimize } \|z\|_1, \text{ subject to:} \\ & z = z_i + \partial w + \sum_{j \in T_i} \alpha_j z_j, \\ & w \in C_q(X_{b_i}), \\ & \alpha_j \in \mathbb{k}, \\ & \text{where } T_i = \{j \mid b_j < b_i < d_j\}. \end{aligned}$$

4. VOLUME OPTIMAL CYCLE

In this section, we propose volume optimal cycles, a new tool to characterize generators appearing in persistent homology. In this section, we will show the generalized version of volume optimal cycles and the computation algorithm. The limited version of volume optimal cycles shown in [16] will be explained in the next section.

We assume Condition 1 and consider the filtration $\mathbb{X} : \emptyset = X_0 \subset \dots \subset X_K = X$. A *persistent volume* for $(b_i, d_i) \in D_q(\mathbb{X})$ is defined as follows.

Definition 2. $z \in C_{q+1}(X)$ is a *persistent volume* for $(b_i, d_i) \in D_q(\mathbb{X})$ if z satisfies the following conditions:

$$(10) \quad z = \sigma_{d_i} + \sum_{\sigma_k \in \mathcal{F}_{q+1}} \alpha_k \sigma_k,$$

$$(11) \quad \tau^*(\partial z) = 0 \text{ for all } \tau \in \mathcal{F}_q,$$

$$(12) \quad \sigma_{b_i}^*(\partial z) \neq 0,$$

where $\mathcal{F}_q = \{\sigma_k : q\text{-simplex} \mid b_i < k < d_i\}$, $\{\alpha_k \in \mathbb{k}\}_{\sigma_k \in \mathcal{F}_{q+1}}$, and σ_k^* is the dual basis of cochain $C^q(X)$, i.e. σ_k^* is the linear map on $C_q(X)$ satisfying $\sigma_k^*(\sigma_j) = \delta_{kj}$ for any $\sigma_k, \sigma_j : q\text{-simplex}$.

⁶ In fact, in [15], two slightly different algorithms are shown, and this algorithm is one of them.

Note that the persistent volume is defined only if the death time is finite.

The *volume optimal cycle* for (b_i, d_i) and the *optimal volume* for the pair are defined as follows.

Definition 3. $\partial \hat{z}$ is the volume optimal cycle and \hat{z} is the optimal volume for $(b_i, d_i) \in D_q(\mathbb{X})$ if \hat{z} is the solution of the following optimization problem.

$$\text{minimize } \|z\|_0, \text{ subject to (10), (11), and (12).}$$

The following theorem ensures that the optimization problem of the volume optimal cycle always has a solution.

Theorem 4. *There is always a persistent volume of any $(b_i, d_i) \in D_q(\mathbb{X})$.*

The following theorem ensures that the volume optimal cycle is good to represent the homology generator corresponding to (b_i, d_i) .

Theorem 5. *Let $\{x_j \mid j = 1, \dots, p\}$ be all persistence cycles for $D_q(\mathbb{X})$. If z_i is a persistent volume of $(b_i, d_i) \in D_q(\mathbb{X})$, $\{x_j \mid j \neq i\} \cup \{\partial z_i\}$ are also persistence cycles for $D_q(\mathbb{X})$.*

Intuitively say, a homology generator is dead by filling the internal volume of a ring, a cavity, etc., and a persistent volume is such an internal volume. The volume optimal cycle minimize the internal volume instead of the size of the cycle.

Proof of Theorem 4. Let z_i be a persistence cycle satisfying (3-6). Since

$$z_i \in B_q(X_{d_i}) \setminus B_q(X_{d_i-1}),$$

we can write z_i as follows.

$$(13) \quad \begin{aligned} z_i &= \partial(w_0 + w_1), \\ w_0 &= \sigma_{d_i} + \sum_{\sigma_k \in \mathcal{F}_{q+1}} \alpha_k \sigma_k, \\ w_1 &= \sum_{\sigma_k \in \mathcal{G}_{q+1}} \alpha_k \sigma_k, \end{aligned}$$

where $\mathcal{G}_{q+1} = \{\sigma_k : (q+1)\text{-simplex} \mid k < b_i\}$. Note that the coefficient of σ_{d_i} in w_0 can be normalized as in (13). Now we prove that w_0 is a persistent volume. From $z_i \in Z_q(X_{b_i})$ and $\partial w_1 \in C_q(X_{b_i-1})$, we have $\partial w_0 = z_i - \partial w_1 \in C_q(X_{b_i})$ and this means that $\tau^*(\partial w_0) = 0$ for all $\tau \in \mathcal{F}_q$. From $\partial w_1 \in C_q(X_{b_i-1})$, we have $\sigma_{b_i}^*(\partial w_1) = 0$ and therefore $\sigma_{b_i}^*(\partial w_0) = \sigma_{b_i}^*(z_i)$, and the right hand side is not zero since $z_i \in Z_q(X_{b_i}) \setminus Z_q(X_{b_i-1}) \subset C_q(X_{b_i}) \setminus C_q(X_{b_i-1})$. Therefore w_0 satisfies all conditions (10-12). \square

Proof of Theorem 5. We prove the following arguments. The theorem follows from these arguments.

$$\begin{aligned} \partial z_i &\in Z_q(X_{b_i}) \setminus Z_q(X_{b_i-1}), \\ \partial z_i &\in B_q(X_{d_i}) \setminus B_q(X_{d_i-1}). \end{aligned}$$

The condition (11), $\tau^*(\partial z_i) = 0$ for all $\tau \in \mathcal{F}_q$, means $\partial z_i \in Z_q(X_{b_i})$. The condition (12), $\sigma_{b_i}^*(\partial z_i) \neq 0$, means $\partial z_i \notin Z_q(X_{b_i-1})$. Since $\partial z_i = \partial \sigma_{d_i} + \sum_{\sigma_k \in \mathcal{F}_{q+1}} \alpha_k \partial \sigma_k$, and $B_q(X_{d_i}) = B_q(X_{d_i-1}) \oplus \langle \partial \sigma_{d_i} \rangle$, we have $\partial z_i \in B_q(X_{d_i}) \setminus B_q(X_{d_i-1})$ and this finishes the proof. \square

4.1. Algorithm for volume optimal cycles. To compute the volume optimal cycles, we can apply the same strategies as optimal cycles. Using linear programming with \mathbb{R} coefficient and ℓ^1 norm is efficient and gives sufficiently good results. Using integer programming is slower, but it gives better results.

Now we remark the condition (12). In fact it is impossible to handle this condition by linear/integer programming directly. We need to replace this condition to $|\sigma_{b_i}^*(\partial z)| \geq \epsilon$ for sufficiently small $\epsilon > 0$ and we need to solve the optimization problem twice for $\sigma_{b_i}^*(\partial z) \geq \epsilon$ and $\sigma_{b_i}^*(\partial z) \leq -\epsilon$. However, as mentioned later, we can often remove the constraint (12) to solve the problem and this fact is useful for faster computation.

We can also apply the following heuristic performance improvement technique to the algorithm for an alpha filtration by using the locality of an optimal volume. The simplices which contained in the optimal volume for (b_i, d_i) , are contained in a neighborhood of σ_{d_i} . Therefore we take a parameter $r > 0$, and we use $\mathcal{F}_q^{(r)} = \{\sigma \in \mathcal{F}_q \mid \sigma \subset B_r(\sigma_{d_i})\}$ instead of \mathcal{F}_q to reduce the size of the optimization problem, where $B_r(\sigma_{d_i})$ is the ball of radius r whose center is the centroid of σ_{d_i} . Obviously, we cannot find a solution with a too small r . In Algorithm 2, r is properly chosen by a user but the computation software can automatically increase r when the optimization problem cannot find a solution.

We also use another heuristic for faster computation. To treat the constraint (12), we need to apply linear programming twice for positive case and negative case. In many examples, the optimized solution automatically satisfies (12) even if we remove the constrain. There is an example in which the corner-cutting does not work (shown in 4.2), but it works well in many cases. One way is that we try to solve the linear programming without (12) and check the (12), and if (12) is satisfied, output the solution. Otherwise, we solve the linear programming twice with (12).

The algorithm to compute a volume optimal cycle for an alpha filtration is Algorithm 2.

Algorithm 2 Algorithm for a volume optimal cycle

procedure VOLUME-OPTIMAL-CYCLE(\mathbb{X}, r)

 Compute the persistence diagram $D_q(\mathbb{X})$

 Choose a birth-death pair $(b_i, d_i) \in D_q(\mathbb{X})$ by a user

 Solve the following optimization problem:

 minimize $\|z\|_1$, subject to:

$$z = \sigma_{d_i} + \sum_{\sigma_k \in \mathcal{F}_{q+1}^{(r)}} \alpha_k \sigma_k,$$

$$\tau^*(\partial z) = 0 \text{ for all } \tau \in \mathcal{F}_q^{(r)}.$$

if we find the optimal solution \hat{z} **then**

if $\sigma_{b_i}^*(\partial \hat{z}) \neq 0$ **then**

return \hat{z} and $\partial \hat{z}$

else

 Retry optimization twice with the additional constrain:

$$\sigma_{b_i}^*(\partial z) \geq \epsilon \text{ or } \sigma_{b_i}^*(\partial z) \leq -\epsilon$$

else

return the error message to the user to choose larger r .

If your filtration is not an alpha filtration, possibly you cannot use the locality technique. However, in that case, the core part of the algorithm works fine and you can use the algorithm.

4.2. Some properties about volume optimal cycles. In this subsection, we remark some properties about volume optimal cycles.

First, the volume optimal cycle for a birth-death pair is not unique. Figure 6 shows such an example. In this example, $D_1 = \{(1, 5), (3, 4), (2, 6)\}$ and both (b) and (c) is the optimal volumes of the birth-death pair (2, 6). In this filtration, any weighted sum of (b) and (c) with weight λ and $1 - \lambda$ ($0 \leq \lambda \leq 1$) in the sense of chain complex is the volume optimal cycle of (2, 6) if we use \mathbb{R} as a coefficient and ℓ^1 norm. However, standard linear programming algorithms choose an extremal point solution, hence the algorithms choose either $\lambda = 0$ or $\lambda = 1$ and our algorithm outputs either (b) or (c).

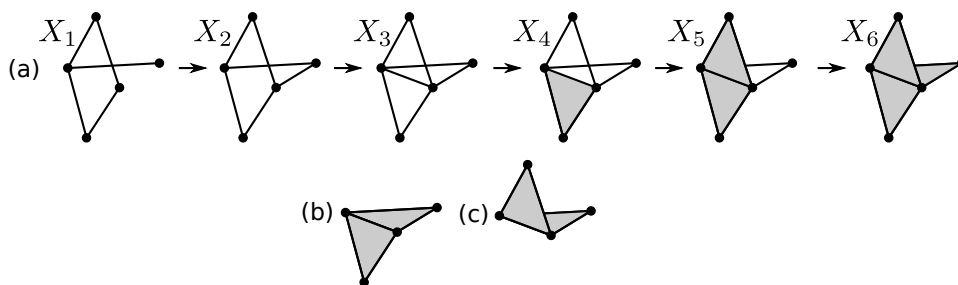


FIGURE 6. An example of non-unique volume optimal cycles.

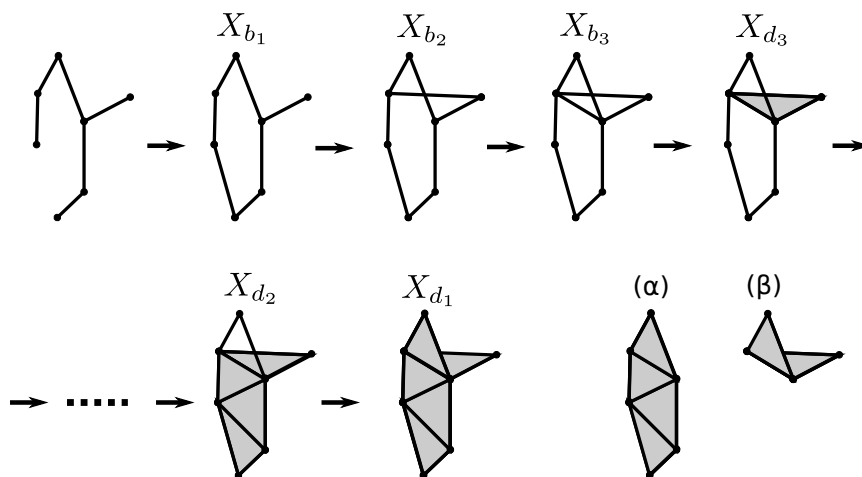


FIGURE 7. An example of the failure of the computation of the volume optimal cycle if the constrain (12) is removed.

Second, by the example in Fig 7, we show that the optimization problem for the volume optimal cycle may give a wrong solution if the constrain (12) is removed. In this example, $(b_1, d_1), (b_2, d_2), (b_3, d_3)$ are birth-death pairs in the 1st PD, and the volume optimal cycle for (b_1, d_1) is (α) in Fig. 7, but the algorithm gives (β) if the constrain (12) is removed.

5. VOLUME OPTIMAL CYCLE ON $(n - 1)$ -TH PERSISTENT HOMOLOGY

In this section, we consider a triangulation of a convex set in \mathbb{R}^n and its $(n - 1)$ -th persistent homology. More precisely, we assume the following conditions.

Condition 6. *A simplicial complex X in \mathbb{R}^n satisfies the following conditions.*

- Any k -simplex ($k < n$) in X is a face of an n -simplex
- $|X|$ is convex

For example, an alpha filtration satisfies the above conditions if the point cloud has more than n points and satisfies the general position condition. In addition, we assume Condition 1 to simplify the statements of results and algorithms.

The thesis [16] pointed out that $(n - 1)$ -th persistent homology is isomorphic to 0th persistent cohomology of the dual filtration by the Alexander duality under the assumption. By using this fact, the thesis defined volume optimal cycles under different formalization from ours. The thesis defined a volume optimal cycle as an output of Algorithm 3. In fact, the two definitions of volume optimal cycles are equivalent on $(n - 1)$ -th persistent homology. 0th persistent cohomology is deeply related to the connected components, and we can compute the volume optimal cycle by linear computation cost. The thesis also pointed out that $(n - 1)$ -th persistent homology has a tree structure called persistence trees (or PH trees).

In this section, we always use \mathbb{Z}_2 as a coefficient of homology since using \mathbb{Z}_2 makes the problem easier.

The following theorems hold.

Theorem 7. *The optimal volume for $(b_i, d_i) \in D_{n-1}(\mathbb{X})$ is uniquely determined.*

Theorem 8. *If z_i and z_j are the optimal volumes for two different birth-death pairs (b_i, d_i) and (b_j, d_j) in $D_{n-1}(\mathbb{X})$, one of the followings holds:*

- $z_i \cap z_j = \emptyset$,
- $z_i \subset z_j$,
- $z_i \supset z_j$.

Note that we can naturally regard any $z = \sum_{\sigma: n\text{-simplex}} k_\sigma \sigma \in C_n(X)$ as a subset of n -simplices of X , $\{\sigma : n\text{-simplex} \mid k_\sigma \neq 0\}$, since we use \mathbb{Z}_2 as a homology coefficient.

From Theorem 8, we know that $D_{n-1}(\mathbb{X})$ can be regarded as a forest (i.e. a set of trees) by the inclusion relation. The trees are called *persistence trees*.

We can compute all optimal volumes and persistence trees on $D_{n-1}(\mathbb{X})$ by the merge tree algorithm (Algorithm 3). This algorithm is a modified version of the algorithm in [16]. To describe the algorithm, we prepare a directed graph (V, E) where V is a set of nodes and E is a set of edges. In the algorithm, an element of V is a n -cell in $X \cup \{\sigma_\infty\}$ and an element of E is a directed edge between two n -cells, where $\sigma_\infty = \mathbb{R}^n \setminus X$ is the n -cell in the one point compactification space $\mathbb{R}^n \cup \{\infty\} \simeq S^n$. An edge has extra data in \mathbb{Z} and we write the edge from σ to τ with extra data k as $(\sigma \xrightarrow{k} \tau)$. Since the graph is always a forest through the whole algorithm, we always find a root of a tree which contains a n -cell σ in the graph (V, E) by recursively following edges from σ . We call this procedure $\text{ROOT}(\sigma, V, E)$.

The following theorem gives us the interpretation of the result of the algorithm to the persistence information.

Theorem 9. *Let (V, E) be a result of Algorithm 3. Then the followings hold.*

- (i) $D_{n-1}(\mathbb{X}) = \{(b, d) \mid (\sigma_d \xrightarrow{b} \sigma_s) \in E\}$
- (ii) *The optimal volume for (b, d) is all descendant nodes of σ_d in (E, V)*

Algorithm 3 Computing persistence trees by merge-tree algorithm

```

procedure COMPUTE-TREE( $\mathbb{X}$ )
  initialize  $V = \{\sigma_\infty\}$  and  $E = \emptyset$ 
  for  $k = K, \dots, 1$  do
    if  $\sigma_k$  is a  $n$ -simplex then
      add  $\sigma_k$  to  $V$ 
    else if  $\sigma_k$  is a  $(n - 1)$ -simplex then
      let  $\sigma_s$  and  $\sigma_t$  are two  $n$ -cells whose common face is  $\sigma_k$ 
       $\sigma_{s'} \leftarrow \text{ROOT}(\sigma_s, V, E)$ 
       $\sigma_{t'} \leftarrow \text{ROOT}(\sigma_t, V, E)$ 
      if  $s' = t'$  then
        continue
      else if  $s' > t'$  then
        Add  $(\sigma_{t'} \xrightarrow{k} \sigma_{s'})$  to  $E$ 
      else
        Add  $(\sigma_{s'} \xrightarrow{k} \sigma_{t'})$  to  $E$ 
  return  $(V, E)$ 

```

(iii) The persistence trees is computable from (E, V) . That is, (b_i, d_i) is a child of (b_j, d_j) if and only if there are edges $\sigma_{d_i} \xrightarrow{b_i} \sigma_{d_j} \xrightarrow{b_j} \sigma_s$.

The theorems in this section can be proven from the following facts:

- From Alexander duality, for a simplicial complex X in \mathbb{R}^n ,

$$H_q(X) \simeq H^{n-q-1}((\mathbb{R}^n \setminus X) \cup \{\infty\}),$$

holds.

- ∞ is required for one point compactification of \mathbb{R}^n .
- More precisely, we use the dual decomposition of X .
- By applying above Alexander duality to a filtration, $(n - 1)$ -th persistent homology is isomorphic to 0-th persistent cohomology of the dual filtration.
- On a cell complex \bar{X} , a basis of 0-th cohomological vector space is given by

$$\left\{ \sum_{\sigma \in C} \sigma^* \mid C \in \text{cc}(\bar{X}) \right\},$$

where $\text{cc}(\bar{X})$ is the connected component decomposition of 0-cells in \bar{X} .

- Merge-tree algorithm traces the change of connectivity in the filtration, and it gives the structure of 0-the persistent cohomology.

We prove the theorems in Appendix A.

5.1. Computation cost for merge-tree algorithm. In the algorithm, we need to find the root from its descendant node. The naive way to find the root is following the graph step by step to the ancestors. In the worst case, the time complexity of the naive way is $O(N)$ where N is the number of n -simplices, and total time complexity of the algorithm becomes $O(N^2)$. The union-find algorithm [21] is used for a similar data structure, and we can apply the idea of union-find algorithm. By adding a shortcut path to the root in a similar way as the union-find algorithm, the amortized time complexity is improved to almost constant time⁷. Using the technique, the total time complexity of the Algorithm 3 is $O(N)$.

⁷ More precisely, the amortized time complexity is bounded by the inverse of Ackermann function and it is less than 5 if the data size is less than $2^{2^{2^{16}}}$. Therefore we can regard the time complexity as constant.

6. COMPARISON BETWEEN VOLUME OPTIMAL CYCLES AND OPTIMAL CYCLES

In this section, we compare volume optimal cycles and optimal cycles. In fact, optimal cycles and volume optimal cycles are identical in many cases. However, since we can use optimal volumes in addition to volume optimal cycles, we have more information than optimal cycles. One of the most prominent advantage of volume optimal cycles is children birth-death pairs, explained below.

6.1. Children birth-death pairs. In the above section, we show that there is a tree structure on an $(n-1)$ -th persistence diagram computed from a triangulation of a convex set in \mathbb{R}^n . Unfortunately, such a tree structure does not exist in a general case. However, in the research of amorphous solids by persistent homology[7], a hierarchical structure of rings in \mathbb{R}^3 is effectively used, and it will be helpful if we can find such a structure on a computer. In [7], the hierarchical structure was found by computing all optimal cycles and searching multiple optimal cycles which have common vertices. However, computing all optimal cycles or all volume optimal cycles is often expensive as shown in Section 7.4 and we require a cheaper method. The optimal volume is available for that purpose. When the optimal volume for a birth-death pair (b_i, d_i) is $\hat{z} = \sigma_{d_i} + \sum_{\sigma_k \in \mathcal{F}_{q+1}} \hat{\alpha}_k \sigma_k$, the *children birth-death pairs* of (b_i, d_i) is defined as follows:

$$\{(b_j, d_j) \in D_q(\mathbb{X}) \mid \sigma_{d_j} \in \mathcal{F}_{q+1}, \hat{\alpha}_{d_j} \neq 0\}.$$

This is easily computable from a optimal volume with low computation cost.

Now we remark that if we consider $(n-1)$ -th persistent homology in \mathbb{R}^n , the children birth-death pairs of $(b_i, d_i) \in D_{n-1}(\mathbb{X})$ is identical to all descendants of (b_i, d_i) in the tree structure. This fact is known from Theorem 8. This fact suggests that we can use children birth-death pairs as a good substitute for the tree structure appearing on $D_{n-1}(\mathbb{X})$ in \mathbb{R}^n . The ability of children birth-death pairs is shown in Section 7.2, the example of amorphous silica.

6.2. Some examples in which volume optimal cycles and optimal cycles are different. We show some differences between optimal cycles and volume optimal cycles on a filtration. In Fig 8, the 1st PD of this filtration is $\{(2, 5), (3, 4)\}$. The optimal cycle of $(3, 4)$ is z_1 since $\|z_1\|_1 < \|z_2\|_1$ but the volume optimal cycle is z_2 . In this example, z_2 is better than z_1 to represent the birth-death pair $(3, 4)$. The example is deeply related to Theorem 5. Such a theorem does not hold for optimal cycles and it means that an optimal cycle may give misleading information about a birth-death pair. This is one advantage of volume optimal cycles compared to optimal cycles.

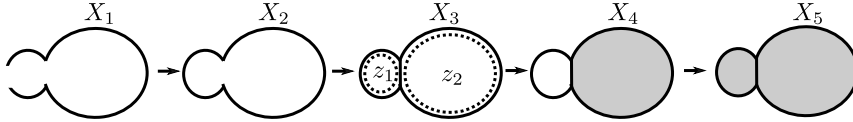


FIGURE 8. A filtration whose optimal cycle and volume optimal cycle are different.

In Fig. 9 and Fig. 10, optimal cycles and volume optimal cycles are also different. In Fig. 9, the optimal cycle is z_1 but the volume optimal cycle z_2 . In Fig. 10, the optimal cycle for $(3, 4)$ is z_1 but the volume optimal cycle is $z_1 + z_2$.

In Fig 11, the 1st PD is $(2, \infty)$ and we cannot define the volume optimal cycle but can define the optimal cycle. In general, we cannot define the volume optimal cycle for a birth-death pair with infinite death time. If we use an alpha filtration in \mathbb{R}^n , such a problem does not occur because a Delaunay triangulation is always

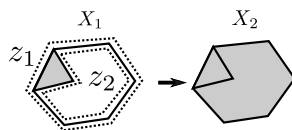


FIGURE 9. Another filtration whose optimal cycle and volume optimal cycle are different.

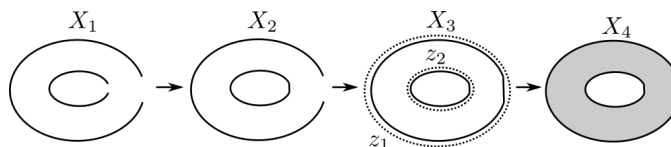


FIGURE 10. Another filtration whose optimal cycle and volume optimal cycle are different.

acyclic. But if we use another type of a filtration, we possibly cannot use volume optimal cycles. That may be a disadvantage of volume optimal cycles if we use a filtration other than an alpha filtration, such as a Vietoris-Rips filtration.

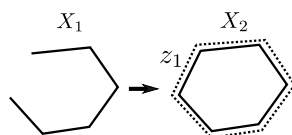


FIGURE 11. A filtration without a volume optimal cycle.

One more advantage of the volume optimal cycles is the simplicity of the computation algorithm. For the computation of the optimal cycles we need to keep track of all persistence cycles but for the volume optimal cycles we need only birth-death pairs. Some efficient algorithms implemented in `phat` and `dipha` do not keep track of such data, hence we cannot use such softwares to compute the optimal cycles without modification. By contrast we can use such softwares for the computation of the volume optimal cycles.

7. EXAMPLE

In this section, we will show the example results of our algorithm. In all of these examples, we use alpha or weighted alpha filtrations.

For all of these examples, optimal volumes and volume optimal cycles are computed on a laptop PC with 1.2 GHz Intel(R) Core(TM) M-5Y71 CPU and 8GB memory on Debian 9.1. `Dipha` [5] is used to compute PDs, `CGAL`⁸ is used to compute (weighted) alpha filtrations, and `Clp` [22] is used to solve the linear programming. Python is used to write the program and `pulp`⁹ is used for the interface to `Clp` from python. `Paraview`¹⁰ is used to visualize volume optimal cycles.

If you want to use the software, please contact with us. `Homcloud`¹¹, a data analysis software with persistent homology developed by our laboratory, provides the algorithms shown in this paper. `Homcloud` provides the easy access to the volume optimal cycles. We can visualize the volume optimal cycle of a birth-death pair only by clicking the pair in a PD on `Homcloud`'s GUI.

⁸<http://www.cgal.org/>

⁹<https://github.com/coin-or/pulp>

¹⁰<https://www.paraview.org/>

¹¹http://www.wpi-aimr.tohoku.ac.jp/hiraoka_lab/research-english.html

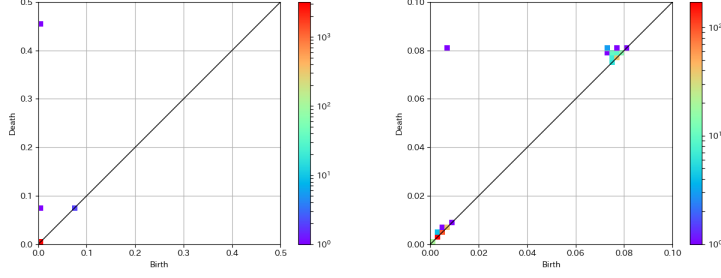


FIGURE 12. The 1st and 2nd PDs of the point cloud on a torus.

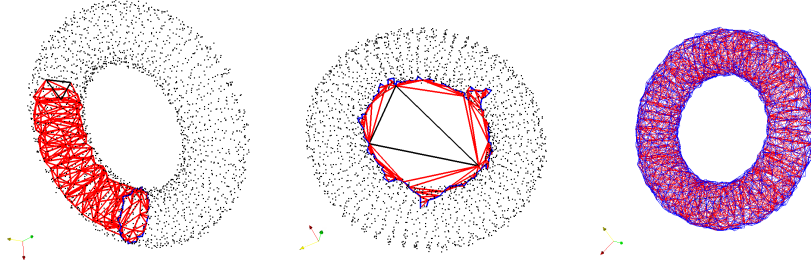


FIGURE 13. Volume optimal cycles for $(0.001, 0.072)$ and $(0.001, 0.453)$ in D_1 and $(0.008, 0.081)$ in D_2 on the torus point cloud.

7.1. 2-dimensional Torus. The first example is a 2-dimensional torus in \mathbb{R}^3 . 2400 points are randomly scattered on the torus and PDs are computed. Figure 12 shows the 1st and 2nd PDs. The 1st PD has two birth-death pairs $(0.001, 0.072)$ and $(0.001, 0.453)$ and the 2nd PD has one birth-death pair $(0.008, 0.081)$ far from the diagonal. These birth-death pairs correspond to generators of $H_1(\mathbb{T}^2) \simeq \mathbb{k}^2$ and $H_2(\mathbb{T}^2) \simeq \mathbb{k}$.

Figure 13 shows the volume optimal cycles of these three birth-death pairs using Algorithm 2. Blue lines show volume optimal cycles, red lines show optimal volumes, black lines show σ_d for each birth death pair (b, d) (we call this simplex the *death simplex*). Black dots show the point cloud. By the figure, we understand how homology generators appear and disappear in the filtration of the torus point cloud. The computation times are 25sec, 33sec, and 7sec on our laptop PC.

By using Algorithm 3, we can also compute volume optimal cycles in D_2 . In this example, the computation time by Algorithm 3 is about 2sec. This is much faster than Algorithm 2 even if Algorithm 3 computes *all* volume optimal cycles.

7.2. Amorphous silica. In this example, we use the atomic configuration of amorphous silica computed by molecular dynamical simulation as a point cloud and we try to reproduce the result in [7]. In this example, we use weighted alpha filtration whose weights are the radii of atoms. The number of atoms are 8100, 2700 silicon atoms and 5400 oxygen atoms.

Figure 1 shows the 1st PD. This diagram have four characteristic areas C_P , C_T , C_O , and B_O . These areas correspond to the typical ring structures in the amorphous silica as follows. Amorphous silica consists of silicon atoms and oxygen atoms and the network structure is build by covalent bonds between silicons and

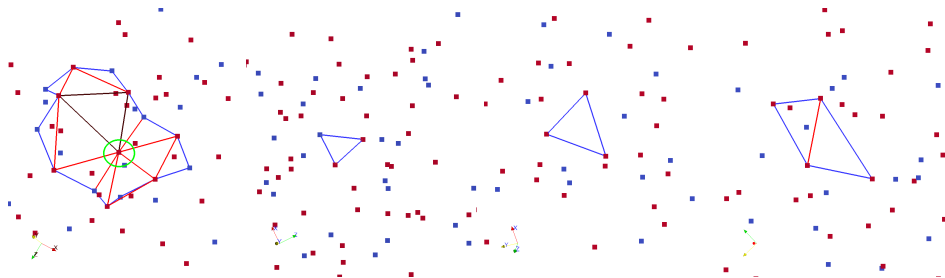


FIGURE 14. Volume optimal cycles in amorphous silica in C_P , C_T , C_O , and B_O (from left to right).

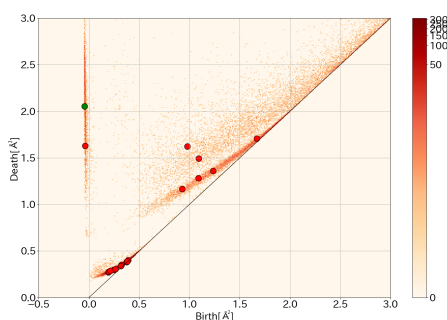


FIGURE 15. Children birth-death pairs. Red circles are children birth-death pairs of the green birth-death pair.

oxygens. C_P has rings whose atoms are $\cdots -\text{Si}-\text{O}-\text{Si}-\text{O}-\cdots$ where $-$ is a covalent bond between a silicon atom and a oxygen atom. C_P has triangles consisting of $\text{O}-\text{Si}-\text{O}$. C_O has triangles consisting of three oxygen atoms appearing alternately in $\cdots -\text{O}-\text{Si}-\text{O}-\text{Si}-\text{O}-\cdots$. B_O has many types of ring structures, but one typical ring is a quadrangle consists of four oxygen atoms appearing alternately in $\cdots -\text{O}-\text{Si}-\text{O}-\text{Si}-\text{O}-\text{Si}-\text{O}-\cdots$.

Figure 14 shows the volume optimal cycles for birth-death pairs in C_P , C_t , C_O and B_O . In this figure oxygen (red) and silicon (blue) atoms are also shown in addition to volume optimal cycles, optimal volumes, and death simplices. We can reproduce the result of [7] about ring reconstruction.

We also know that the oxygen atom rounded by the green circle in this figure is important to determine the death time. The death time of this birth-death pair is determined by the radius of circumcircle of the black triangle (the death simplex), hence if the oxygen atom moves away, the death time becomes larger. The oxygen atom is contained in another $\cdots -\text{Si}-\text{O}-\text{Si}-\text{O}-\cdots$ ring structure around the volume optimal cycle (the blue ring). By the analysis of the optimal volume, we clarify that such an interaction of covalent bond rings determines the death times of birth-death pairs in C_P . This analysis is impossible for the optimal cycles, and the volume optimal cycles enable us to analyze persistence diagrams more deeply.

Figure 15 shows the children birth-death pairs of the green birth-death pair. The rings corresponding to these children birth-death pairs are subrings of the large ring corresponding to the green birth-death pair. This computation result shows that a ring in C_P has subrings in C_T , C_O , and B_O . The hierarchical structure of these rings shown in [7]. We can easily find such a hierarchical structure by using our new algorithm.

The computation time is 3 or 4 seconds for each volume optimal cycle on the laptop PC. The computation time for amorphous silica is much less than that for 2-torus even if the number of points in amorphous silica is larger than that in 2-torus. This is because the locality of volume optimal cycles works very fine in the example of amorphous silica.

7.3. Face centered cubic lattice with defects. The last example uses the point cloud of face centered cubic (FCC) lattice with defects. By this example, we show how to use the persistence trees computed by Algorithm 3. The point cloud is prepared by constructing perfect FCC lattice, adding small Gaussian noise to each point, and randomly removing points from the point cloud.

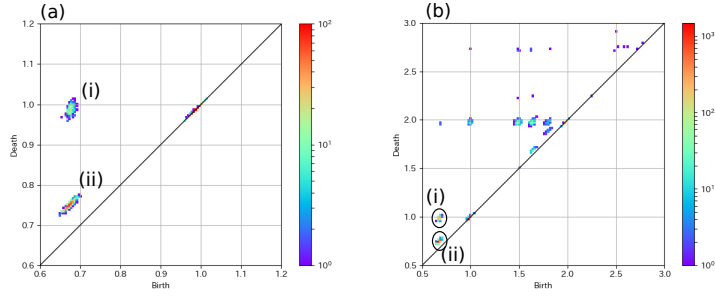


FIGURE 16. (a) The 2nd PD of the perfect FCC lattice with small Gaussian noise. (b) The 2nd PD of the lattice with defects.

Figure 16(a) shows the 2nd PD of FCC lattice with small Gaussian noise. (i) and (ii) in the figure correspond to octahedron and tetrahedron cavities in the FCC lattice. In materials science, these cavities are famous as octahedron sites and tetrahedron sites. Figure 16(b) shows the 2nd PD of the lattice with defects. In the PD, birth-death pairs corresponding to octahedron and tetrahedron cavities remain ((i) and (ii) in Fig 16(b)), but other types of birth-death pairs appear in this PD. These pairs correspond to other types of cavities generated by removing points from the FCC lattice.

Figure 17(a) shows a tree computed by Algorithm 3. Red markers are nodes of the tree, and lines between two markers are edges of the tree, where upper left nodes are ancestors and lower right nodes are descendants. The tree means that the largest cavity corresponding to most upper-left node has sub cavities corresponding descendant nodes. Figure 17(b) shows the volume optimal cycle of the most upper-left node, (c) shows the volume optimal cycles of pairs in (i), and (d) shows the volume optimal cycles of pairs in (ii). Using the algorithm, we can study the hierarchical structures of the 2nd PH.

7.4. Computation performance comparison with optimal cycles. We compare the computation performance between optimal cycles and volume optimal cycles. We use OptiPers for the computation of optimal cycles for persistent homology, which is provided by Dr. Escobar, one of the authors of [15]. OptiPers is written in C++ and our software is mainly written in python, and python is much slower than C++, so the comparison is not fair, but suggestive for the readers.

We use two test data. One test data is the atomic configuration of amorphous silica used in the above example. The number of points is 8100. Another data is the partial point cloud of the amorphous silica. The number of points is 881. We call these data the large data and the small data. Table 1 shows the computation time of optimal cycles/volume optimal cycles for all birth-death pairs in the 1st PD by OptiPers/Homcloud.

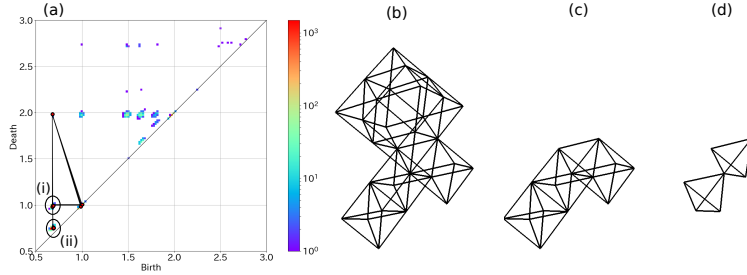


FIGURE 17. A persistence tree and related volume optimal cycles. (a) The persistence tree whose root is $(0.68, 1.98)$. (b) The volume optimal cycle of the root pair. (c) The volume optimal cycles of birth-death pairs in (i) which are descendants of the root pair. (d) The volume optimal cycles of birth-death pairs in (ii) which are descendants of the root pair.

| | optimal cycles (OptiPers) | volume optimal cycles (Homcloud) |
|----------------|---------------------------|----------------------------------|
| the small data | 1min 17sec | 3min 9sec |
| the large data | 5hour 46min | 4hour 13min |

TABLE 1. Computation time of optimal cycles and volume optimal cycles on the large/small data.

For the small data, OptiPers is faster than Homcloud, but to the contrary, for the large data, Homcloud is faster than OptiPers. This is because the performance improvement technique using the locality of the optimal volume works fine for the large data, but for the small data the technique is not so effective and the overhead cost using python is dominant for Homcloud. This benchmark shows that the volume optimal cycles have an advantage about the computation time when an input point cloud is large.

8. CONCLUSION

In this paper, we propose the idea of volume optimal cycles to identify good geometric realizations of homology generators appearing in persistent homology. Optimal cycles are proposed for that purpose in [15], but our method is faster for large data and gives better information. Especially, we can reasonably compute children birth-death pairs only from a volume optimal cycle. Volume optimal cycles are already proposed under the limitation of dimension in [16], and this paper generalize the idea.

Our idea and algorithm are widely applicable to and useful for the analysis of point clouds in \mathbb{R}^n by using the (weighted) alpha filtrations. Our method gives us intuitive understanding of PDs. In [23], such inverse analysis from a PD to its original data is effectively used to study many geometric data with machine learning on PDs and our method is useful to the combination of persistent homology and machine learning.

In this paper, we only treat simplicial complex, but our method is also applicable to a cell filtration and a cubical filtration. Our algorithms will be useful to study sublevel or superlevel filtrations given by 2D/3D digital images.

APPENDIX A. PROOFS OF SECTION 5

The theorems shown in this section are a kind of folklore theorems. Some researchers about persistent homology probably know the fact that the merge-tree algorithm gives a 0th PD, and the algorithm is available to compute an $(n - 1)$ -th PD using Alexander duality, but we cannot find the literature for the complete proof. [16] stated that the algorithm also gives the tree structure on an $(n - 1)$ -th PD, but the thesis does not have the complete proof. Therefore we will show the proofs here.

Alexander duality says that for any good topological subspace X of S^n , the $(k - 1)$ -th homology of X and $(n - k)$ -th cohomology of $S^n \setminus X$ have the same information. In this section, we show Alexander duality theorem on persistent homology. In this section, we always use \mathbb{Z}_2 as a coefficient of homology and cohomology.

A.1. Persistent cohomology. The persistent cohomology is defined on a decreasing sequence $\mathbb{Y} : Y_0 \supset \cdots \supset Y_K$ of topological spaces. The cohomology vector spaces and the linear maps induced from inclusion maps define the sequence

$$H^q(Y_0) \rightarrow \cdots \rightarrow H^q(Y_K),$$

and this family of maps is called persistent cohomology $H^q(\mathbb{Y})$. The decomposition theorem also holds for persistent cohomology in the same way as persistent homology and we define the q th cohomologous persistence diagram $D^q(\mathbb{Y})$ using the decomposition.

A.2. Alexander duality. Before explaining Alexander duality, we show the following proposition about the dual decomposition.

Proposition 10. *For any oriented closed n -manifold S and its simplicial decomposition K , there is a decomposition of M , \bar{K} , satisfying the followings:*

- (1) \bar{K} is a cell complex of M .
- (2) There is a one-to-one correspondence between K and \bar{K} . For $\sigma \in K$, we write the corresponding cell in \bar{K} as $\bar{\sigma}$.
- (3) $\dim \sigma = n - \dim \bar{\sigma}$ for any $\sigma \in K$.
- (4) If $X \subset K$ a subcomplex of K ,

$$\bar{X} = \{\bar{\sigma} \mid \sigma \notin X\}$$

is a subcomplex of \bar{K} .

- (5) We consider the chain complex of K and \bar{K} , let ∂ and $\bar{\partial}$ be boundary operators on those chain complexes, and let B and \bar{B} be matrix representations of ∂ and $\bar{\partial}$, i.e. $\partial\sigma_i = \sum_j B_{ji}\sigma_j$ and $\bar{\partial}\bar{\sigma}_i = \sum_j \bar{B}_{ji}\bar{\sigma}_j$. Then \bar{B} is the transpose of B .

This decomposition \bar{K} is called the *dual decomposition* of K . One example of the dual decomposition is a Voronoi decomposition with respect to a Delaunay triangulation. Using the dual decomposition, we can define the map θ from $C_k(K)$ to $C^{n-k}(\bar{K})$ for $k = 0, \dots, n$ as the linear extension of $\sigma_i \mapsto \bar{\sigma}_i^*$, where $\{\sigma_i\}_i$ are k -simplices of K , $\{\bar{\sigma}_i\}_i$ are corresponding $(n - k)$ -cells of \bar{K} , and $\{\bar{\sigma}_i^* \in C^{n-k}(\bar{K})\}_i$ is the dual basis of $\{\bar{\sigma}_i\}_i$.

The map θ satisfies the equation

$$(14) \quad \theta \circ \partial = \delta \circ \theta,$$

where δ is the coboundary operator on $C^*(\bar{K})$ from Proposition 10. The map θ induces the isomorphism $H_k(K) \simeq H^{n-k}(\bar{K})$, and the isomorphism is called Poincaré duality.

Using the dual decomposition, we show Alexander duality theorem.

Theorem 11. For an n -sphere S^n , its simplicial decomposition K , and a subcomplex of $X \subset K$, we take a dual decomposition \bar{K} and a subcomplex of \bar{X} as in Proposition 10. Then,

$$(15) \quad \tilde{H}_{k-1}(X) \simeq \tilde{H}^{n-k}(\bar{X})$$

holds for any $k = 1, \dots, n$, where \tilde{H} is the reduced (co)-homology.

To apply the duality theorem to persistent homology, we investigate that isomorphism in detail.

First, we consider the case of $K = X$. In this case, $\bar{X} = \emptyset$ and the homology of X is the same as an n -sphere. Therefore, $\tilde{H}_k(X) = 0$ for any $k = 0, \dots, n-1$ and this is isomorphic to $\tilde{H}^{n-k-1}(\emptyset) = 0$.

Next, we consider the case that $K \neq X$. In this case, there is a n -simplex of K which is not contained in X . We write the n -simplex as ω and let K_0 be $K \setminus \{\omega\}$.

Proposition 12. There is the following isomorphism.

$$(16) \quad H_k(K, X) \simeq H^{n-k}(\bar{X}).$$

This isomorphism is induced by:

$$\begin{aligned} \bar{\theta} : C_k(K, X) = C_k(K)/C_k(X) &\rightarrow C^{n-k}(\bar{X}) \\ \sum_{i=s+1}^t a_i \sigma_i + C_k(X) &\mapsto \sum_{i=s+1}^t a_i \bar{\sigma}_i^* \end{aligned}$$

where $\{\sigma_1, \dots, \sigma_t\}$ is all k -simplices of K and $\{\sigma_1, \dots, \sigma_s\}$ is all k -simplices of X .

The map θ is well-define and isomorphic since $\{\bar{\sigma}_{s+1}, \dots, \bar{\sigma}_t\}$ is equal to the set of all $(n-k)$ -simplices of \bar{X} . In addition, $\delta \circ \bar{\theta} = \bar{\theta} \circ \partial$ holds where ∂ is the boundary operator on $C_*(K, X)$, and δ is the coboundary operator on $C^*(\bar{X})$ due to (14). Using the map θ , the isomorphism $\bar{\theta}_* : H_k(K, X) \rightarrow H^{n-k}(\bar{X})$ is defined as follows,

$$(17) \quad \left[\sum_{i=s+1}^t a_i \sigma_i + C_k(X) \right] \mapsto \left[\sum_{i=s+1}^t a_i \bar{\sigma}_i^* \right].$$

The next key is the long exact sequence on the pair (K, X) .

$$(18) \quad \dots \rightarrow \tilde{H}_k(X) \rightarrow \tilde{H}_k(K) \xrightarrow{j_*} H_k(K, X) \xrightarrow{\partial_*} \tilde{H}_{k-1}(X) \rightarrow \tilde{H}_{k-1}(K) \rightarrow \dots$$

The map ∂_* is written as follows

$$(19) \quad \partial_*([z + C_k(X)]) = [\partial z],$$

and j_* is induced by the projection map from $C_k(K)$ to $C_k(K, X)$. If $k \neq n$, since both $\tilde{H}_k(K)$ and $\tilde{H}_{k-1}(K)$ are zero, The following map is isomorphic due to the long exact sequence (18).

$$(20) \quad \partial_* : H_k(K, X) \xrightarrow{\sim} H_{k-1}(K).$$

By combining (16) and (20), we conclude the isomorphism (16) for $k \neq n$. We can explicitly write the isomorphism from \tilde{H}^{n-k} to \tilde{H}_{k-1} as follows using (17) and (19):

$$(21) \quad \left[\sum_{i=s+1}^t a_i \bar{\sigma}_i^* \right] \mapsto \left[\partial \left(\sum_{i=s+1}^t a_i \bar{\sigma}_i \right) \right].$$

When $k = n$, we need to treat the problem more carefully. From the long exact sequence (18), we can show that the following sequence is exact:

$$(22) \quad \begin{array}{ccccccc} H_n(X) & \rightarrow & H_n(K) & \xrightarrow{j_*} & H_n(K, X) & \xrightarrow{\partial_*} & H_{n-1}(X) \rightarrow H_{n-1}(K) \\ \parallel & & \parallel & & \parallel & & \parallel \\ 0 & & \mathbb{Z}_2 & & & & 0 \end{array} .$$

Let $\{\sigma_1, \dots, \sigma_{t-1}, \sigma_t = \omega\}$ be n -simplices of K and $\{\sigma_1, \dots, \sigma_s\}$ be n -simplices of X . From the assumption of $X \neq K$, $s < t$ holds. It is easy to show that $\tau = \sigma_1 + \dots + \sigma_t$ is the generator of $Z_n(K)$. From the definition of the reduced cohomology,

$$(23) \quad \tilde{H}^0(\bar{X}) = Z^0(\bar{X}) / \langle \bar{\tau} \rangle,$$

where $Z^0(\bar{X}) = \ker(\delta : C^0(\bar{X}) \rightarrow C^1(\bar{X}))$ and $\bar{\tau} = \bar{\theta}(j(\tau)) = \bar{\sigma}_{s+1}^* + \dots + \bar{\sigma}_t^*$. For \mathbb{Z}_2 coefficient, the following set is the basis of $Z^0(\bar{X})$

$$(24) \quad \left\{ \sum_{\bar{\sigma} \in C} \bar{\sigma}^* \mid C \in \text{cc}(\bar{X}) \right\},$$

where $\text{cc}(\bar{X})$ is the connected component decomposition of 0-cells in \bar{X} . Therefore, we can write $\tilde{H}^0(\bar{X})$ as:

$$\tilde{H}^0(X) = \left\{ \left[\sum_{\bar{\sigma} \in C} \bar{\sigma}^* \right] \mid C \in \text{cc}_\omega(\bar{X}) \right\},$$

where $\text{cc}_\omega(\bar{X}) \subset \text{cc}(\bar{X})$ is the set of connected components which do not contain $\bar{\omega}$. Using the above relations, we can show $\tilde{H}^0(\bar{X}) \simeq H_{n-1}(X)$ whose isomorphism is the linear extension of the following:

$$(25) \quad \begin{aligned} \Theta : \tilde{H}^0(X) &\rightarrow H_{n-1}(X) \\ \Theta\left(\left[\sum_{\bar{\sigma} \in C} \bar{\sigma}^* \right]\right) &= \left[\partial \left(\sum_{\bar{\sigma} \in C} \sigma \right) \right] \\ &\text{for all } C \in \text{cc}_\omega(\bar{X}). \end{aligned}$$

A.3. Alexander duality and persistent homology. To apply Alexander duality to the persistent homology, we need to consider the relation between inclusion maps and the isomorphism θ_* . For two subcomplex $X_1 \subset X_2$ of K , the following diagram commutes:

$$(26) \quad \begin{array}{ccc} C_\ell(K, X_1) & \xrightarrow{\bar{\theta}} & C^{n-\ell}(\bar{X}_1) \\ \downarrow \phi & & \downarrow \bar{\phi}^\vee \\ C_\ell(K, X_2) & \xrightarrow{\bar{\theta}} & C^{n-\ell}(\bar{X}_2), \end{array}$$

where ϕ and $\bar{\phi}^\vee$ are induced from the inclusion maps. Note that $X_1 \subset X_2$ induces $\bar{X}_1 \supset \bar{X}_2$ and $\bar{\phi}^\vee$ is defined from $C^{n-\ell}(\bar{X}_1)$ to $C^{n-\ell}(\bar{X}_2)$. Using (26), we have the following commutative diagram:

$$(27) \quad \begin{array}{ccc} H_\ell(K, X_1) & \xrightarrow{\bar{\theta}_*} & H^{n-\ell}(\bar{X}_1) \\ \downarrow \phi_* & & \downarrow \bar{\phi}^* \\ H_\ell(K, X_2) & \xrightarrow{\bar{\theta}_*} & H^{n-\ell}(\bar{X}_2), \end{array}$$

We also have the following commutative diagram between two long exact sequences (28)

$$(28) \quad \begin{array}{ccccccccccc} \cdots & \longrightarrow & \tilde{H}_k(X_1) & \longrightarrow & \tilde{H}_k(K) & \xrightarrow{j_*} & H_k(K, X_1) & \xrightarrow{\partial_*} & \tilde{H}_{k-1}(X_1) & \longrightarrow & \cdots \\ & & \downarrow \phi_* & & \parallel & & \downarrow \phi_* & & \downarrow \phi_* & & \\ \cdots & \longrightarrow & \tilde{H}_k(X_2) & \longrightarrow & \tilde{H}_k(K) & \xrightarrow{j_*} & H_k(K, X_2) & \xrightarrow{\partial_*} & \tilde{H}_{k-1}(X_2) & \longrightarrow & \cdots \end{array}$$

From (27), (28), and the discussion in Section A.2, we have the following commutative diagram:

$$\begin{array}{ccc} \tilde{H}_{\ell-1}(X_2) & \xrightarrow{\sim} & \tilde{H}^{n-\ell}(\bar{X}_2) \\ \downarrow \phi_* & & \downarrow \bar{\phi}_* \\ \tilde{H}_{\ell-1}(X_1) & \xrightarrow{\sim} & \tilde{H}^{n-\ell}(\bar{X}_1). \end{array}$$

This diagram means that the isomorphism preserves the decomposition structure of persistent homology and hence $\tilde{H}_{\ell-1}(\mathbb{X}) \simeq \tilde{H}^{n-\ell}(\bar{\mathbb{X}})$ holds for $\mathbb{X} : X_0 \subset \cdots \subset X_K$ where $\bar{\mathbb{X}} : \bar{X}_0 \supset \cdots \supset \bar{X}_K$.

A.4. Alexander duality and a triangulation in \mathbb{R}^n . Here, we consider the simplicial filtration in \mathbb{R}^n satisfying Condition 6. Under the condition, we need to embed the filtration \mathbb{X} on \mathbb{R}^n into S^n by using one point compactification. We consider an embedding $|X| \rightarrow S^n$ and take σ_∞ as $S^n \setminus |X|$. Using the embedding, we can regard $X \cup \{\sigma_\infty\}$ as a cell decomposition of S^n . The above discussion about Alexander duality on persistent homology works on this cell complex, if we properly define the boundary operator and the dual decomposition. In that case, we regard σ_∞ as ω in the definition of K_0 .

A.5. Merge-Tree Algorithm for 0th Persistent Cohomology. The above discussion shows that all we need to do is to give an algorithm for computing 0th persistent cohomology of the dual filtration. In fact, we can efficiently compute the 0th cohomologous persistence diagram using the following merge-tree algorithm.

To simplify the explanation of the algorithm, we assume the following condition. This condition corresponds to Condition 1 for persistent homology.

Condition 13.

- $Y = \{\bar{\sigma}_1, \dots, \bar{\sigma}_K, \bar{\sigma}_\infty\}$ is a cell complex and $Y_k = \{\bar{\sigma}_{k+1}, \dots, \bar{\sigma}_K, \bar{\sigma}_\infty\}$ is a subcomplex of Y for any $0 \leq k < K$.
- $\bar{\sigma}_\infty$ is 0-cell and $Y_K = \{\bar{\sigma}_\infty\}$ is also a subcomplex of Y .
- Y is connected.

Under the condition, we explain the algorithm to compute the decomposition of 0th persistence cohomology on the decreasing filtration $\mathbb{Y} : Y = Y_0 \supset \cdots \supset Y_K = \{\bar{\sigma}_\infty\}$.

Algorithm 4 computes the 0th cohomologous persistence diagram. In this algorithm, (V_k, E_k) is a graph whose nodes are 0-cells of Y and whose edges have extra data in \mathbb{Z} . Later we show this algorithm is applicable for computing $D_{n-1}(\mathbb{X})$ using Alexander duality.

This algorithm tracks all $\{(V_k, E_k)\}_{k=0, \dots, K}$ for the mathematical proof, but when you implement the algorithm, you do not need to keep the history and you can directly update the set of nodes and edges.

Theorem 14. *The 0th reduced cohomologous persistence diagram $\tilde{D}^0(\mathbb{Y})$ is given as follows:*

$$\tilde{D}^0(\mathbb{Y}) = \{(k, s) \mid (\bar{\sigma}_s \xrightarrow{k} \bar{\sigma}_t) \in E_0\}$$

To prove the theorem and justify the algorithm, we show some basic facts about the graph (V_k, E_k) given by the algorithm. These facts are shown by checking the edges/nodes adding rule of each step in Algorithm 4.

Fact 15. $V_k = \{\bar{\sigma}_\ell : 0\text{-simplex in } Y \mid k < \ell\}$

Fact 15 is obvious from the algorithm.

Algorithm 4 Merge-Tree algorithm for the 0th cohomologous PD

```

procedure COMPUTE-TREE( $\mathbb{Y}$ )
  initialize  $V_K = \{\bar{\sigma}_\infty\}$  and  $E_K = \emptyset$ 
  for  $k = K, \dots, 1$  do
    if  $\bar{\sigma}_k$  is a 0-simplex then
       $V_{k-1} \leftarrow V_k \cup \{\bar{\sigma}_k\}$ ,  $E_{k-1} \leftarrow E_k$ 
    else if  $\bar{\sigma}_k$  is a 1-simplex then
      let  $\bar{\sigma}_s, \bar{\sigma}_t$  are two endpoints of  $\bar{\sigma}_k$ 
       $\bar{\sigma}_{s'} \leftarrow \text{ROOT}(\bar{\sigma}_s, V_k, E_k)$ 
       $\bar{\sigma}_{t'} \leftarrow \text{ROOT}(\bar{\sigma}_t, V_k, E_k)$ 
      if  $s' = t'$  then
         $V_{k-1} \leftarrow V_k$ ,  $E_{k-1} \leftarrow E_k$ 
      else if  $s' > t'$  then
         $V_{k-1} \leftarrow V_k$ ,  $E_{k-1} \leftarrow E_k \cup \{(\bar{\sigma}_{t'} \xrightarrow{k} \bar{\sigma}_{s'})\}$ 
      else
         $V_{k-1} \leftarrow V_k$ ,  $E_{k-1} \leftarrow E_k \cup \{(\bar{\sigma}_{s'} \xrightarrow{k} \bar{\sigma}_{t'})\}$ 
    else
       $V_{k-1} \leftarrow V_k$ ,  $E_{k-1} \leftarrow E_k$ 
  return  $(V_0, E_0)$ 

```

Fact 16. For any k , (V_k, E_k) is a forest, i.e. a set of trees. That is, the followings hold:

- There is no loop in the graph
- For any node, the number of outgoing edges from the node is zero or one.
 - If the number is zero, the node is a root node
 - If the number is one, the node is a child node

We can inductively prove Fact 16 since an edge is added between two roots of (V_k, E_k) in the algorithm.

Fact 17. The topological connectivity of Y_k is the same as (V_k, T_k) . That is, $\{\bar{\sigma}_{i_1}, \dots, \bar{\sigma}_{i_\ell}\}$ is all 0-simplices of a connected component in X_k if and only if there is a tree in (V_k, E_k) whose nodes are $\{\bar{\sigma}_{i_1}, \dots, \bar{\sigma}_{i_\ell}\}$.

This is because the addition of a node to the graph corresponds to the addition of a connected component in \mathbb{Y} and the addition of an edge corresponds to the concatenation of two connected components.

Fact 18. If there is a path $\bar{\sigma}_s \xrightarrow{k} \bar{\sigma}_t \rightarrow \dots \rightarrow \bar{\sigma}_{s'} \xrightarrow{k'} \bar{\sigma}_{t'}$ in $(V_{k''}, E_{k''})$, the following inequality holds:

$$k' < k < s < s'.$$

Proof of Fact 18. The edge $\bar{\sigma}_s \xrightarrow{k} \bar{\sigma}_t$ is added after $\bar{\sigma}_{s'} \xrightarrow{k'} \bar{\sigma}_{t'}$ is added in the algorithm since any edge is added between two root nodes, hence we have $k' < k$. We also show that $k < s < t$ and $k' < s' < t'$ from the rule of edge addition and this inequalities hold for any intermediate edge in the path, so we have $s < s'$. The required inequality comes from these inequalities. \square

The following fact is shown since in the algorithm each edge is added between two root nodes.

Fact 19. If $\bar{\sigma}_s$ is not a root of a tree in (V_k, E_k) , the subtree whose root node is $\bar{\sigma}_s$ does not change in the sequence of graphs: $(V_k, E_k) \subset \dots \subset (V_0, E_0)$.

Using these facts, we set up the 0th persistence cohomology. We prepare some symbols:

$$\begin{aligned}
R_k &= \{\bar{\sigma}_s \mid \bar{\sigma}_s \text{ is a root of a tree in } (V_k, E_k)\}, \\
\text{desc}_k(\bar{\sigma}_s) &= \{\bar{\sigma}_t \mid \bar{\sigma}_t \text{ a descendant node of } \bar{\sigma}_s \text{ in } (V_k, E_k), \text{ including } \bar{\sigma}_s \text{ itself}\}, \\
\overline{\text{desc}}_k(\bar{\sigma}_s) &= \{\bar{\sigma}_t \in \text{desc}_0(\bar{\sigma}_s) \mid k \leq t\}, \\
y_s^{(k)} &= \sum_{\bar{\sigma}_t \in \text{desc}_k(\bar{\sigma}_s)} \bar{\sigma}_t^* \in C^0(Y_k), \\
\hat{y}_s^{(k)} &= \sum_{\bar{\sigma}_t \in \overline{\text{desc}}_k(\bar{\sigma}_s)} \bar{\sigma}_t^* \in C^0(Y_k), \\
\bar{\varphi}_k^\vee : C^0(Y_k) &\rightarrow C^0(Y_{k+1}) : \text{the induced map of the inclusion map } Y_k \hookrightarrow Y_{k+1}.
\end{aligned}$$

We prove the following lemma.

Lemma 20. $\{\hat{y}_s^{(k)} \mid \bar{\sigma}_s \in R_k\}$ is a basis of $Z^0(Y_k) = H^0(Y_k)$.

Proof. From Fact 17 and the theory of 0th cohomology, we have that $\{y_s^{(k)} \mid \bar{\sigma}_s \in R_k\}$ are basis of $H^0(Y_k)$. Here, we prove the following three facts. Then the theory of linear algebra leads the statement of the lemma.

- (i) $\#\{y_s^{(k)} \mid \bar{\sigma}_s \in R_k\} = \#\{\hat{y}_s^{(k)} \mid \bar{\sigma}_s \in R_k\} = \#R_k$
 - (ii) Any $\hat{y}_s^{(k)}$ for $\bar{\sigma}_s \in R_k$ is a linear sum of $\{y_s^{(k)} \mid \bar{\sigma}_s \in R_k\}$
 - (iii) $\{\hat{y}_s^{(k)} \mid \bar{\sigma}_s \in R_k\}$ are linearly independent.
- (i) is trivial. We show (ii). We can write $\hat{y}_s^{(k)}$ explicitly by using the two graphs (V_k, E_k) and (V_0, E_0) by the following way. Let $R_k(\bar{\sigma}_s)$ be

$$R_k(\bar{\sigma}_s) = \{\bar{\sigma}_t \in R_k \mid \bar{\sigma}_t \text{ is a descendant of } \bar{\sigma}_s \text{ in } (V_0, E_0), \text{ including } \bar{\sigma}_s \text{ itself}\}.$$

Then we write $\hat{y}_s^{(k)} = \sum_{\bar{\sigma}_t \in R_k(\bar{\sigma}_s)} x_t^{(k)}$. We can show the equation from the followings.

- The family $\{\text{desc}_k(\bar{\sigma}_s) \mid \bar{\sigma}_s \in R_k\}$ is pairwise disjoint.
- $\overline{\text{desc}}_k(\bar{\sigma}_s) = \bigsqcup_{\bar{\sigma}_t \in R_k(\bar{\sigma}_s)} \text{desc}_k(\bar{\sigma}_t)$

The first one comes from Fact 17. Next $\overline{\text{desc}}(\bar{\sigma}_s) \supset \bigsqcup_{\bar{\sigma}_t \in R_k(\bar{\sigma}_s)} \text{desc}_k(\bar{\sigma}_t)$ is shown. Pick any $\bar{\sigma}_u \in \text{desc}_k(\bar{\sigma}_t)$ with $\bar{\sigma}_t \in R_k(\bar{\sigma}_s)$. Then there are a path $\bar{\sigma}_u \rightarrow \cdots \rightarrow \bar{\sigma}_t$ in (V_k, E_k) and a path $\bar{\sigma}_t \rightarrow \cdots \rightarrow \bar{\sigma}_s$ in (V_0, E_0) . Since (V_k, E_k) is a subgraph of (V_0, E_0) , there is a path from $\bar{\sigma}_u$ to $\bar{\sigma}_s$ in (V_0, E_0) through $\bar{\sigma}_t$ and this means that $\bar{\sigma}_u \in \overline{\text{desc}}_k(\bar{\sigma}_s)$. To show the inverse inclusion relation, we pick any $\bar{\sigma}_u$ in $\overline{\text{desc}}_k(\bar{\sigma}_s)$. Since $\bar{\sigma}_u \in V_k$, there is $\bar{\sigma}_t \in R_k$ such that $\bar{\sigma}_u \in \text{desc}_k(\bar{\sigma}_t)$. There are a path $\bar{\sigma}_u \rightarrow \cdots \rightarrow \bar{\sigma}_s \in (V_0, E_0)$ and $\bar{\sigma}_u \rightarrow \cdots \rightarrow \bar{\sigma}_t \in (V_k, E_k)$. Since (V_k, E_k) is a subgraph of (V_0, E_0) and there is a unique path from a node to a root node in a tree, there is always the node $\bar{\sigma}_t$ in the path $\bar{\sigma}_u \rightarrow \cdots \rightarrow \bar{\sigma}_s \in (V_0, E_0)$ and it means that $\bar{\sigma}_t \in R_k(\bar{\sigma}_s)$. We prove $\overline{\text{desc}}_k(\bar{\sigma}_s) = \bigsqcup_{\bar{\sigma}_t \in R_k(\bar{\sigma}_s)} \text{desc}_k(\bar{\sigma}_t)$.

We will show (iii). R_k is ordered as $\{\bar{\sigma}_{s_1}, \dots, \bar{\sigma}_{s_m}\}$ with $s_1 < \dots < s_m$. Assume that

$$(29) \quad \sum_{j=1}^m \lambda_j \hat{y}_{s_j}^{(k)} = 0$$

where $\lambda_j \in \mathbb{Z}_2$ and we show $\lambda_j = 0$ for all j . Now we consider the equation $\sum_{j=1}^m \lambda_j \hat{y}_{s_j}^{(k)}(\bar{\sigma}_{s_m}) = 0$ by applying (29) to $\bar{\sigma}_{s_m}$. Obviously, $\hat{y}_{s_m}^{(k)}(\bar{\sigma}_{s_m}) = 1$ since $\bar{\sigma}_{s_m} \in \overline{\text{desc}}_k(\bar{\sigma}_{s_m})$ and $\hat{y}_{s_j}^{(k)}(\bar{\sigma}_{s_j}) = 0$ for any $1 \leq j < m$ since $\bar{\sigma}_{s_m} \notin \overline{\text{desc}}_k(\bar{\sigma}_{s_j})$ from Fact 18. Therefore we have $\lambda_m = 0$. Repeatedly we can show $\lambda_{m-1} = \dots = \lambda_1 = 0$ in the same way and (iii) is shown. \square

The following lemma is easy to show from the definition of the map.

Lemma 21. *The map $\bar{\varphi}_k^\vee$ satisfies the following:*

$$\bar{\varphi}_k^\vee(\hat{y}_s^{(k)}) = \hat{y}_s^{(k+1)}.$$

We also show the following lemma.

Lemma 22. *If $(\bar{\sigma}_s \xrightarrow{k} \bar{\sigma}_t) \in E_0$, the followings hold:*

- (i) $\hat{y}_s^{(u)} \notin Z^0(Y_k)$ for $u \leq k$
- (ii) $\hat{y}_s^{(u)} \in Z^0(Y_{k+1})$ for $k+1 \leq s$
- (iii) $\hat{y}_s^{(u)} \neq 0$ for $u \leq s$
- (iv) $\hat{y}_s^{(u)} = 0$ for $u \geq s+1$

Proof. Since $\hat{y}_s^{(u)}$ is an element of basis of $Z^0(Y_u)$ due to Lemma 20 for $k+1 \leq u \leq s$, we have (ii). From Fact 18, we have $\text{desc}_0(\bar{\sigma}_s) \subset \{\bar{\sigma}_1, \dots, \bar{\sigma}_s\}$ and so $\overline{\text{desc}}_{s+1}(\bar{\sigma}_s) = \emptyset$, therefore (iv) is true. Since $\bar{\sigma}_s \in \overline{\text{desc}}_u(\bar{\sigma}_s)$ for any $u \leq s$ from the definition of $\overline{\text{desc}}_u(\bar{\sigma})$, we have (iii). From the theory of 0th cohomology, $\hat{y}_s^{(u)} \in Z^0(Y_k)$ if and only if $\overline{\text{desc}}_u(\bar{\sigma}_s)$ is a finite union of connected components. However, from Fact 19,

$$\overline{\text{desc}}_u(\bar{\sigma}_s) = \text{desc}_u(\bar{\sigma}_s) \text{ for } u \leq k$$

from Fact 17 this set is a proper subset of $\text{desc}_u(\bar{\sigma}_v)$ where $\bar{\sigma}_v$ is the root of the tree which has $\bar{\sigma}_s$ as a node. Therefore we have (i). \square

The following theorem is required for the treatment of reduced persistent cohomology.

Lemma 23.

- (i) (V_0, E_0) is a single tree.
- (ii) The root of the single tree is $\bar{\sigma}_\infty$
- (iii) $\bar{\sigma}_\infty$ is a root of a tree in (V_k, E_k) for any k .
- (iv) $\hat{y}_\infty^{(k)} = \sum_{\bar{\sigma}_u: 0\text{-simplex}, u > k} \bar{\sigma}_u^*$
- (v) $\tilde{H}^0(Y_k) = H^0(Y_k) / \langle \hat{y}_\infty^{(k)} \rangle$
- (vi) $\{[y_s^{(k)}]_{\langle \hat{y}_\infty^{(k)} \rangle} \mid s \neq \infty, \sigma_s \in R_k\}$ and $\{[y_s^{(k)}]_{\langle \hat{y}_\infty^{(k)} \rangle} \mid s \neq \infty, \sigma_s \in R_k\}$ are two bases of $\tilde{H}^0(Y_k)$

Proof. (i) comes from the connectivity of Y in Condition 13 and Fact 17. (ii) and (iii) comes from Fact 18. (iv) comes from the definition of $\hat{y}_\infty^{(k)}$ and (ii). (v) comes from (iv) and from the definition of reduced cohomology (23). Finally, we conclude (vi) by (i-v). \square

Lemma 20, 21, 22, and 23 lead Theorem 14.

A.6. Merge-tree algorithm for $(n-1)$ -th persistent homology.

Proof of Theorem 9(i). We prove Theorem 9. Theorem 9(i) is the direct result of Theorem 14 and $\tilde{H}_{\ell-1}(\mathbb{X}) \simeq \tilde{H}^{n-\ell}(\tilde{\mathbb{X}})$ by applying Algorithm 4 to $\mathbb{X}^+ : X_0 \subset X_1 \subset \dots \subset X_K$ in S^n and its dual decomposition $\tilde{\mathbb{X}}^+ : \bar{X}_0 \supset \dots \supset \bar{X}_K = \{\bar{\sigma}_\infty\}$. To apply Theorem 14, we check $\bar{X}_0 = \{\bar{\sigma}_1, \dots, \bar{\sigma}_K, \bar{\sigma}_\infty\}$ is connected and it is true since the dual decomposition is also a decomposition of S^n . \square

Proofs of Theorem 7 and Theorem 9(ii). We show that $x_b^{(d)} = \sum_{\bar{\sigma}_t \in \text{desc}_b(\bar{\sigma}_d)} \sigma_t$ is a persistent volume for a birth-death pair (b, d) . (10) is shown by $\text{desc}_b(\bar{\sigma}_d) \subset \{\bar{\sigma}_{b+1}, \dots, \bar{\sigma}_d\}$ from Fact 18 and $\bar{\sigma}_d \in \text{desc}_b(\bar{\sigma}_d)$ from the definition of $\text{desc}_b(\bar{\sigma}_d)$. (11) and (12) is shown from Lemma 22(i) and (ii), and (25).

To prove the optimality of $x_b^{(d)}$, we show the following claim.

Claim: If x is a persistent volume of (b, d) , $x_b^{(d)} \subset x$ holds.

The claim immediately leads Theorem 7 and Theorem 9(ii). From Theorem 5, $[\partial x]_b$ is well defined and nonzero. By the isomorphism for Alexander duality and Lemma 23(vi), there is $R \subset R_b$ such that

$$[\partial x]_b = \Theta\left(\sum_{\sigma_s \in R} [y_s^{(b)}] \langle \hat{y}_\infty^{(b)} \rangle\right),$$

$$\bar{\sigma}_\infty \notin R.$$

From the relation (25) and the definition of $x_s^{(b)}$,

$$[\partial x_s^{(b)}] = \Theta([y_s^{(b)}] \langle \hat{y}_\infty^{(b)} \rangle)$$

for any s with $\sigma_s \in R_k$. Therefore

$$[\partial x]_b = \sum_{\sigma_s \in R} [\partial x_s^{(b)}]_b,$$

and hence

$$\partial x + \sum_{\sigma_s \in R} \partial x_s^{(b)} \in B_{n-1}(X_b),$$

so there exists $w \in C_n(X_b)$ such that

$$\partial(x + \sum_{\sigma_s \in R} x_s^{(b)} + w) = 0$$

holds. Since X_b is a simplicial complex embedded in \mathbb{R}^n , $Z_n(X_b) = 0$ and

$$x + \sum_{\sigma_s \in R} x_s^{(b)} + w = 0.$$

Since $x, x_s^{(b)} \in \langle \sigma_k : n\text{-simplex} \mid b < k \leq d \rangle$ and $w \in C_n(X_b) = \langle \sigma_k : n\text{-simplex} \mid k < b \rangle$, we have $w = 0$ and

$$x = \sum_{\sigma_s \in R} x_s^{(b)}.$$

From (10), x has always σ_d term and so $\sigma_d \in R$ and finish the proof of the claim. \square

Theorem 8 and Theorem 9(iii) are immediately come from the definition of $x_d^{(b)}$ and properties of the tree structure shown in Section A.5.

ACKNOWLEDGEMENTS

Dr. Nakamura provided the data of the atomic configuration of amorphous silica used in the example. Dr. Escolar provided the computation software for optimal cycles on persistent homology. I thank them.

This work is partially supported by JSPS KAKENHI Grant Number JP 16K17638, JST CREST Mathematics15656429, and Structural Materials for Innovation, Strategic Innovation Promotion Program D72.

REFERENCES

- [1] Gunnar Carlsson. Topology and data. *Bull. Amer. Math. Soc.*, 46:255–308, January 2009.
- [2] Herbert Edelsbrunner and John Harer. *Computational topology: an introduction*. American Mathematical Soc., 2010.
- [3] Herbert Edelsbrunner, David Letscher, and Afra Zomorodian. Topological persistence and simplification. *Discrete & Computational Geometry*, 28(4):511–533, Nov 2002.
- [4] Afra Zomorodian and Gunnar Carlsson. Computing persistent homology. *Discrete & Computational Geometry*, 33(2):249–274, Feb 2005.

- [5] Ulrich Bauer, Michael Kerber, and Jan Reininghaus. Distributed computation of persistent homology. In *Proceedings of the Meeting on Algorithm Engineering & Experiments*, pages 31–38, Philadelphia, PA, USA, 2014. Society for Industrial and Applied Mathematics.
- [6] Ulrich Bauer, Michael Kerber, Jan Reininghaus, and Hubert Wagner. Phat – persistent homology algorithms toolbox. *Journal of Symbolic Computation*, 78:76 – 90, 2017. Algorithms and Software for Computational Topology.
- [7] Yasuaki Hiraoka, Takenobu Nakamura, Akihiko Hirata, Emerson G. Escolar, Kaname Matsue, and Yasumasa Nishiura. Hierarchical structures of amorphous solids characterized by persistent homology. *Proceedings of the National Academy of Sciences*, 113(26):7035–7040, 2016.
- [8] M. Saadatfar, H. Takeuchi, V. Robins, N. Francois, and Y. Hiraoka. Pore configuration landscape of granular crystallization. *Nature Communications*, 8:15082, 2017.
- [9] Takashi Ichinomiya, Ippei Obayashi, and Yasuaki Hiraoka. Persistent homology analysis of craze formation. *Phys. Rev. E*, 95:012504, Jan 2017.
- [10] V. de Silva and R. Ghrist. Coverage in sensor networks via persistent homology. *Algebraic and Geometric Topology*, 7:339–358, 2007.
- [11] Joseph Minhow Chan, Gunnar Carlsson, and Raul Rabadan. Topology of viral evolution. *Proceedings of the National Academy of Sciences*, 110(46):18566–18571, 2013.
- [12] Tamal K. Dey, Anil N. Hirani, and Bala Krishnamoorthy. Optimal homologous cycles, total unimodularity, and linear programming. *SIAM J. Comput.*, 40(4):1026–1044, July 2011.
- [13] Jeff Erickson and Kim Whittlesey. Greedy optimal homotopy and homology generators. In *Proceedings of the Sixteenth Annual ACM-SIAM Symposium on Discrete Algorithms*, SODA ’05, pages 1038–1046, Philadelphia, PA, USA, 2005. Society for Industrial and Applied Mathematics.
- [14] Chao Chen and Daniel Freedman. Hardness results for homology localization. *Discrete & Computational Geometry*, 45(3):425–448, Apr 2011.
- [15] Emerson G. Escolar and Yasuaki Hiraoka. *Optimal Cycles for Persistent Homology Via Linear Programming*, pages 79–96. Springer Japan, Tokyo, 2016.
- [16] B. Schweinhart. *Statistical Topology of Embedded Graphs*. PhD thesis, Princeton University, August 2015. <https://web.math.princeton.edu/~bschwein/>.
- [17] Herbert Edelsbrunner and Ernst P. Mücke. Three-dimensional alpha shapes. *ACM Trans. Graph.*, 13(1):43–72, January 1994.
- [18] Herbert Edelsbrunner. Weighted alpha shapes. Technical report, Champaign, IL, USA, 1992.
- [19] Tomasz Kaczynski, Konstantin Mischaikow, and Marian Mrozek. *Computational Homology*. Springer, 2004.
- [20] A. Tahbaz-Salehi and A. Jadbabaie. Distributed coverage verification in sensor networks without location information. In *2008 47th IEEE Conference on Decision and Control*, pages 4170–4176, Dec 2008.
- [21] Zvi Galil and Giuseppe F. Italiano. Data structures and algorithms for disjoint set union problems. *ACM Comput. Surv.*, 23(3):319–344, September 1991.
- [22] COIN-OR: Computational Infrastructure for Operations Research. Clp (coin-or linear programming). <https://projects.coin-or.org/Clp>.
- [23] I. Obayashi and Y. Hiraoka. Persistence Diagrams with Linear Machine Learning Models. *ArXiv e-prints*, June 2017.